MinBaS II

Mineral•Ballast• Sten **Område 1** **Rapport nr 1.5.3:01**

MinBaS II Område 1. Produktion och processutveckling
Delområde 1.5 Mineralteknik
Projekt 1.5.3 Bildanalys- Fragmentation Measurement of Bulk Material on Conveyor using 3D Vision

Slutrapport Etapp I

Fragmentation Measurement of Bulk Material on Conveyor using 3D Vision

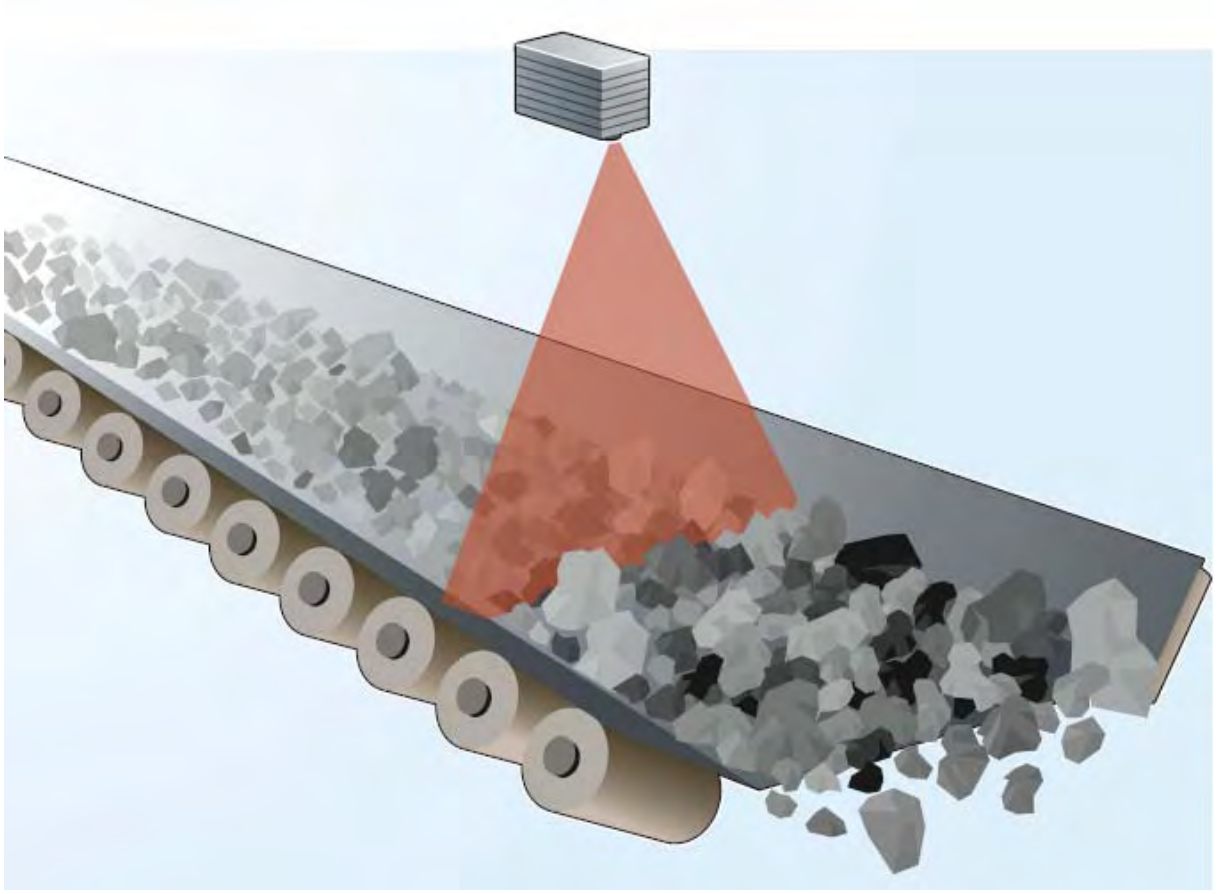

Matthew Thurley & Pär-Erik Martinsson

Luleå Technical University, Computer Science and Electrical Engineering

Luleå 30 June 2009

Contents

Additional Attachments

The following additional attachments are appended to this report.

1. Paper providing the detailed research results entitled *Automated Online Measurement of Particle Size Distribution using 3D Range Data*
2. Paper providing related research involving detection of fines entitled *Fragmentation Size Measurement using 3D Surface Imaging*

Sammanfattning

Projektet har levererat den utlovade proof-of-concept som visar mätsystemets potential. Tester med mätsystemet har genomförts vid Storugns hamn där 3D data insamlades en gång gång per minut under en 13 timmarsperiod vid lastning av två olika storleksfraktioner.

Analysen av data visar att det är möjligt att detektera och spåra förändringar i inkommande storlek. Det är speciellt påtagligt då bytet av fraktioner genomfördes. Analysen visar ett tydligt trendbrott från en stor fraktion till en mindre. Testinstallationen visar också att hårdvaran fungerar, att systemet kan skilja mellan icke-överlappade styckefall från överlappade styckefall. All analys baserades på icke-överlappade styckefall.

Den ekonomiska krisen har direkt påverkat projektets slutfas. På grund av nedgående orderingång lastas för närvarande (Juli 09) väldigt få skepp vid Storugns kalkbrott. Därför har ytterligare mätkampanjer inte kunnat genomföras. Personalneddragningar har haft som följd att det ej heller funnits personal på plats för att bistå genomförande av planerat arbete. Vi har undersökt om Nordkalks avlastningshamn vid SSAB i Luleå kunde användas som mätplats. Oturligt nog skiljer sig hamnarna påtagligt och det var inte möjligt att genomföra de planerade testerna i Luleå.

All hårdvara för en permanent installation är konstruerad och kommer att installeras i Storugn under hösten. Väl på plats kommer vi att undersöka möjligheten att genomföra ytterliga siktningskampanjer för att ytterligare kalibrera mätsystemet.

Inom projektet har vi jämfört skillnader mellan gruvindustri (som vi arbetat med tidigare) och mineralindustri. Det är framförallt två påtagliga skillnader som identifierats. Storleksfördelningarna i mineralindustrin är betydligt smalare vilket bedöms underlätta analysen av data. En annan skillnad är förekomsten av finmaterial. Definitionen av finmaterial är allt material som är mindre än mätsystemets upplösning. Detektering av finmaterial har inte varit nödvändigt för genomförande av projektet men är sannolikt ett område som kräver ytterligare forskning. Exempelvis om tekniken ska användas för optimering av krossar. Lovande resultat rörande detektering av finmaterial presenteras i uppsatsen ”Fragmentation Size Measurements using 3D Surface Imaging”.

För att kunna använda resultaten från steg I av projektet för kvalitetskontroll eller processtyrning krävs ytterligare kvantitativ analys för att säkerställa robustheten och validera storleksbestämningen för fler klasser. Därför föreslås att steg II av projektet genomförs.

Summary

The project has delivered the promised proof-of-concept demonstrating the potential of the measurement system. A site installation of the measurement system was tested collecting 3D surface data once per minute over a 13 hour period during the loading of two different size fractions.

The image processing results are demonstrated to trend in the right direction tracking changes in the material size. Specifically the sizing result is demonstrated to be larger when large rocks are on the conveyor and smaller when small rocks are on the conveyor. Additionally, the test installation has proven that the measurement hardware works, that the system has the ability to distinguish between overlapped and non-overlapped rocks, and produce sizing results for the non-overlapped rocks.

Major reductions in the frequency of ships arriving at Storugn quarry due to the current economic crisis adversely impacted the later part of the project timeline. Furthermore, a reduction in staff has meant that there is currently not someone available to assist us in the sieving lab when a ship does arrive. Additional options for performing the experiments at Nordkalk’s facility in Luleå were explored but the setup does not have a sufficiently similar location at which to perform testing.

The vision hardware for the permanent installation is ready and will now be installed at Storugn on Gotland during the autumn. Once the system is installed options will be explored to ensure that rock samples collected during loading can be sieved as required.

Additionally stage one is considering the differences that may arise in an installation in the aggregates industry where amongst other things, the size range of material is narrower than in mining. A narrower size range is likely to make sizing easier, however, the main consideration is to the presence of fines, that is material below the imaging resolution of the 3D sensor. Detection of fines has not been required in this project, but is likely to be in an aggregates industry application where the goal is crusher control. Some very promising results on fines detection has already been performed in a related project as reported in a paper appended to this report entitled "*Fragmentation Size Measurement using 3D Surface Imaging"*.

The results from stage one were not intended to be used for quality control or process control and this remains the case as they are not yet backed up by the necessary quantitative analysis to ensure a robust, validated sizing for the range of different products relevant to Nordkalk Storugn. A stage two project is proposed to perform this necessary quantitative research and analysis.

Further scoping of the work required for stage two will be performed to clarify the remaining work and aid in planning for stage two. These details will be included in an addendum to this final report after the permanent installation is completed in the autumn.

Fragmentation Measurement of Bulk Material on Conveyor Using 3D Vision

Background

In the mining and aggregate industries a great deal of effort goes into measuring or estimating the size distribution of particulate material. One reason is that suppliers of particulate material are typically paid to supply a specific size range of material. For both industries there is also a key desire for energy efficiency and size quality that is relevant in both crushing and aggregating processes.

Mine and quarry operators want to measure the particle sizing results of all of these activities but sieving is typically impractical as a routine assessment tool due to slow feedback, inconsistent measurement, and time consuming interruption.

As a result there is an opportunity for online, non-contact, fully automated machine vision systems for measurement of particle size that can provide the necessary accuracy and fast feedback to facilitate process control and allow automatic control optimizations for both product size and energy efficiency. This is relevant to a vast range of processes that modify particle size such as blasting, crushing, pelletizing, and in ovens and kilns as shown in Figure 1.

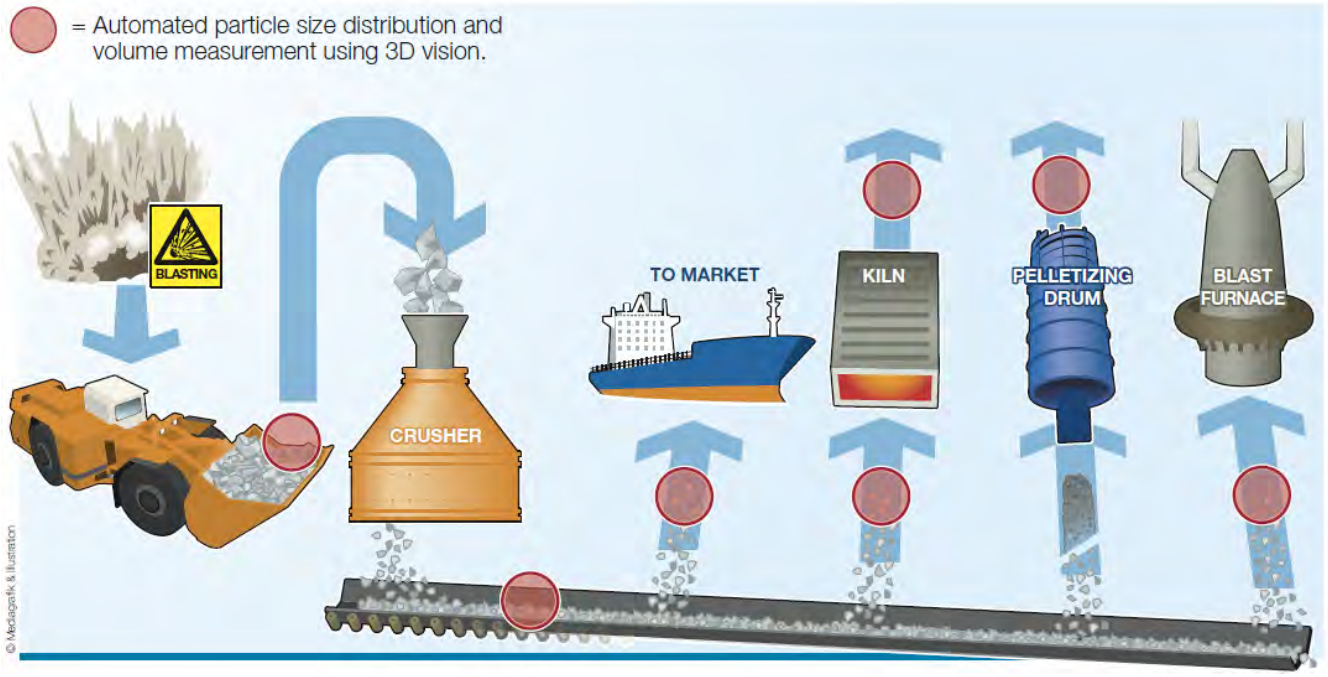

Figure 1: Measurement points for improving quality and efficiency

Nordkalk recognizes this potential and in conjunction with MinBaS II and ProcessIT Innovations supported the installation of a measurement system at their Storugn quarry on Gotland to measure the size of the material during ship loading in real-time. The project has been carried out by Luleå University of Technology, ProcessIT Innovations, and MBV-Systems AB.

Project Results

The detailed research results are provided in an attached paper entitled “Automated Online Measurement of Particle Size Distribution using 3D Range Data”. A short summary of these results is provided here.

A test installation and measurement campaign was performed in late January 2009 collecting data over a 13 hour period. A series of 700 measurements on two separate fractions, 20-40mm and 40-70mm, were collected and image analysis techniques were applied to perform the segmentation and sizing of rock fragments.

The data collected by the system comprises data points spaced approximately 1mm apart in the direction of motion of the belt, and across the belt. This suggests a likely lower limit for particle size detection of 10mm. Material below this will likely appear as fines from the point of view of the measurement system. Information from the quarry manager indicates that on average approximately 10% of the material on the belt will be below 20mm, therefore the presence of fine material will be limited. On rare occasions material in the range 1-5mm or 2-10mm is loaded but this is very uncommon and was not part of the stage one project.

The general image analysis strategy is as follows producing the final sizing results shown in Figure 2. The time of day is shown along the horizontal axis, and the cumulative percent passing is shown on the vertical axis.

1. Segmentation to identify individual fragments in the data
2. Identification of overlapped versus non-overlapped fragments
3. Sizing of individual fragments
4. Map the number of identified fragments by size class to a sieve distribution by weight

What we can see in Figure 2 is that between approximately 22:30 and 01:00 the smaller size fraction 20-40mm product was being loaded. At all other times the 40-70mm product was being loaded.

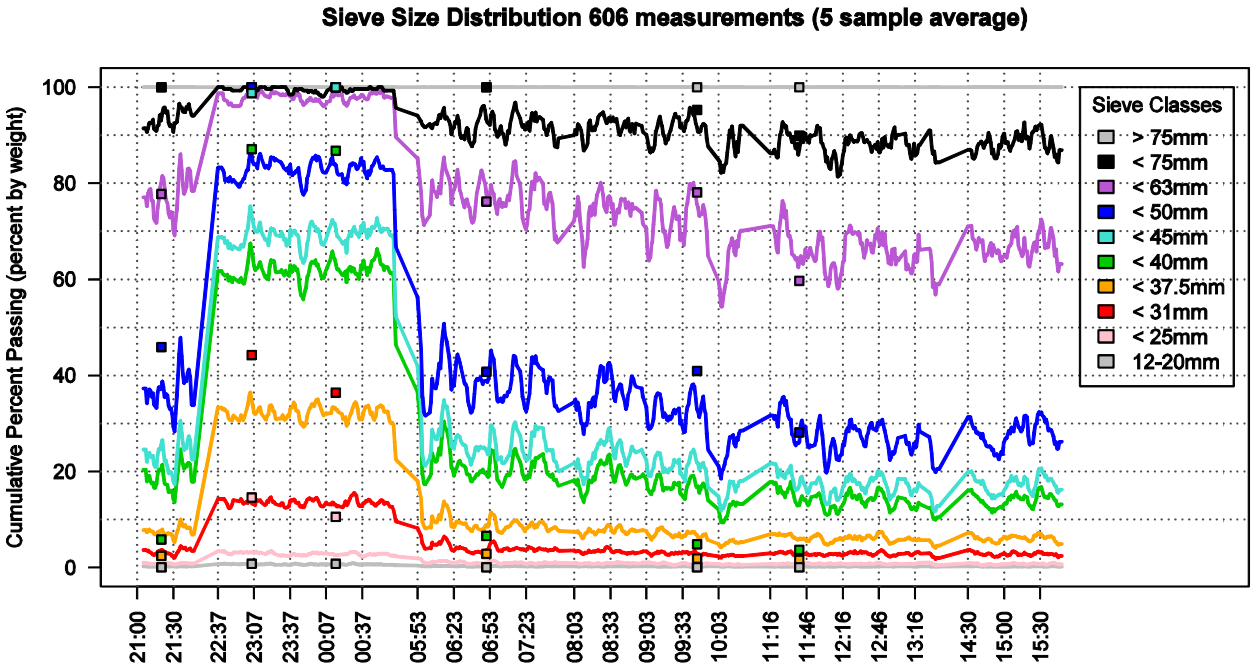

Figure 2: Imaging and sieving results for loading over a 13 hour period

The imaging results are shown to clearly trend in the right direction tracking changes in the material size. For example the green line indicating the proportion of material less than 40mm increases from approximately 20% to 60% in this interval. Furthermore, in the higher size classes, 50, 63, 75, where decision boundaries could be

set for the 40–70mm product independently of the 20–40mm product, the imaging results appear to track the sieving results well. The image analysis overestimates the amount of <40mm size class in the 40–70mm product, by about 10%, and underestimates the cumulative amount in the 20–40mm product by about 25%. Figure 3 shows the cumulative size distribution for the imaging results versus the sieving results at times 0:15 and 6:50 only.

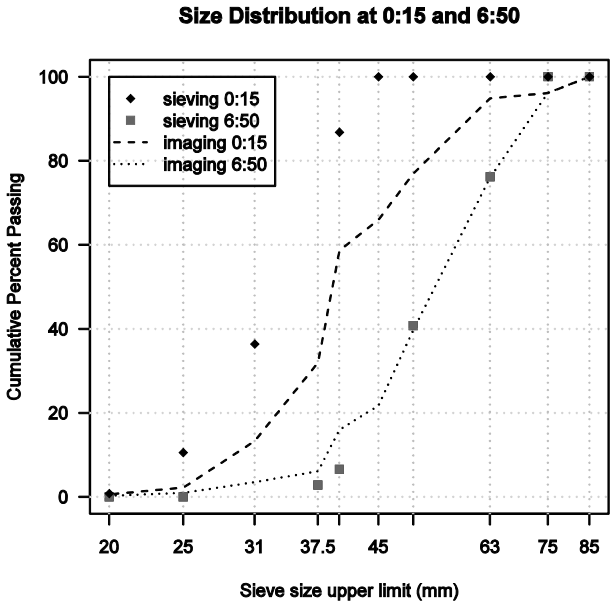

Figure 3: Imaging and sieving results for 2 measurements and sieve results at 0:15 and 6:50

One of the key issues is that size measurement using imaging identifies how many particles are observed of various size classes, but manual sieving measures the weight of particles in each size class. Therefore it is necessary to have a method of mapping from numbers of particles to weight of particles in order to provide a measurement of size that industry understands and can use. In order to achieve this we use an average weight by size class derived from a polynomial fit to the sieving data. This polynomial weight function attempts to produce a reasonable average weight by size class for all cases but further work is necessary to understand this relationship. The sieving data has some inconsistencies with some different average weight results by size class complicated by the use of a different set of sieve decks for the smaller product (20-40mm) than the larger product (40-70mm). Figure 4 shows the average weight data per fragment for all of the sieving results with the polynomial of best fit as a dashed line.

Improvements are expected after performing additional sieving experiments with a much finer sieving, using consistent decks for all products, such as 0, 12, 20, 25, 31, 37, 40, 45, 50, 63, 75 etc. instead of changing the decks as was done here. This sort of high resolution sieving will be carried out in the final sieving trial to collect the necessary field measurements so that we can more accurately represent fragment weight variations by size class. Once this has been achieved we will be better placed to understand whether other factors such as particle shape might also be a source of variation in average fragment weight by size class when considering material from different products.

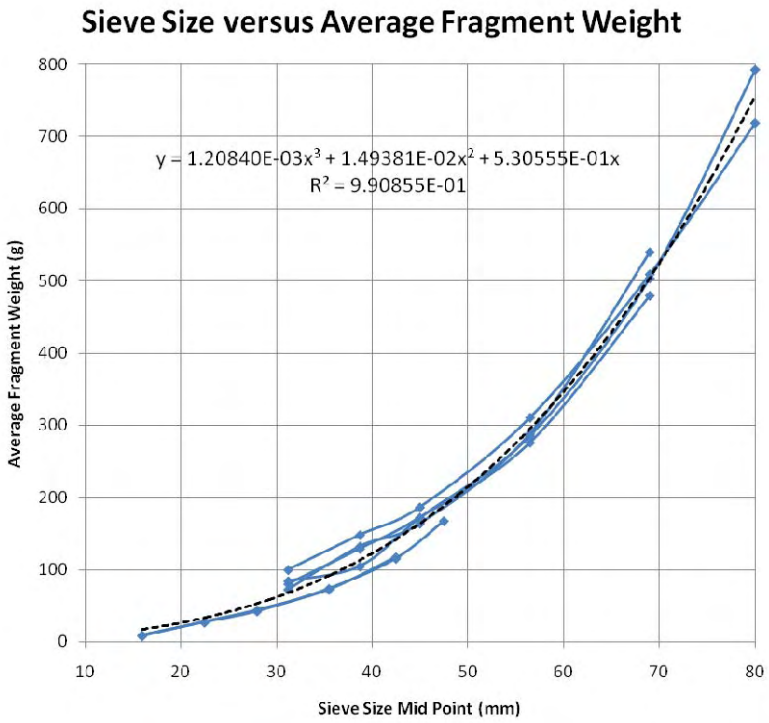

Figure 4: Average fragment weight by size (mid point of sieve size range)

Further work

1. The final installation, sieving and image analysis will be performed in the autumn.
2. Further testing is necessary using a larger size range of products. Specifically imaging data and sieving data need to be collected during the loading of more of the different products produced at the Storugn quarry. This will provide the data necessary to produce a system that can be general to a broad range of products.
3. Characterization of particle shape. The question remains as to whether particles of the same sieve size have different average shape and therefore different average weights based on which product range the particle belongs too. Further sieving results from item 1 above shall clarify whether this is a problem here. Additionally we have some very promising early results on using Fourier series to accurately represent particle size and shape in a rotationally invariant way. Using this sort of information it should be possible to classify particles based on their size and shape, thus identifying which product range it should correspond to and use a more precise average weight for that product range.

Stage 2

Further scoping of the work required for stage two will be performed to clarify the remaining work and aid in planning for stage two. These details will be included in an addendum to this final report after the permanent installation is completed in the autumn.

Automated Online Measurement of Particle Size Distribution using 3D Range Data

Matthew J. Thurley

Luleå University of Technology, Luleå, SE-97187 Sweden (e-mail: matthew.thurley@ltu.se).

Abstract: Fully automated online measurement of the size distribution of limestone fragments on conveyor belt is presented based on 3D range data collected every minute during 13 hours of production. The research establishes the necessary measurement technology to facilitate automatic control of particle breaking or aggregating processes to improve both energy efficiency and product quality. Techniques are presented covering; sizing of fragments, determination of non-overlapped and overlapped fragments, and mapping of sizing results to distributions comparable to sieving. Detailed variations in the product sieve size are shown with an abrupt change when the size range of the limestone fragments was changed.

Keywords: image segmentation, particle size measurement, range data, classification

1. INTRODUCTION

In the mining and aggregate industries a great deal of effort goes into measuring or estimating the size distribution of particulate material. One reason is that suppliers of particulate material are typically paid to supply a specific size range of material. For both industries there is also a key desire for energy efficiency and size quality that is relevant in both crushing and aggregating processes. In addition, blasting and caving are very cost effective methods of rock breakage, but they are not processes that are easily quantified.

Mine and quarry operators want to measure the particle sizing results of all of these activities but sieving is typically impractical as a routine assessment tool due to slow feedback, inconsistent measurement, and time consuming interruption.

As a result there is an opportunity for online, non-contact, fully automated machine vision systems for measurement of particle size that can provide the necessary accuracy and fast feedback to facilitate process control and allow automatic control optimisations for both product size and energy efficiency. This is relevant to a vast range of processes that modify particle size such as blasting, crushing, pelletising, and in ovens and kilns.

There are however, a number of sources of error relevant to techniques that measure only what is visible on the surface of a pile as follows;

Segregation and grouping error, more generally known as the brazil nut effect (Rosato et al., 1987), describes the tendency of the pile to separate into groups of similarly sized particles. It is caused by vibration or motion (for example as rocks are transported by truck or conveyor) with large particles being moved to the surface. It is advisable to measure at a point early on the conveyor before the material has been subjected to excessive vibration and segregation.

Overlapped particle error, describes the fact that many particles are overlapped (see figure 1) and only partially visible and a large bias to the smaller size classes results if they are treated as small non-overlapped and sized using only their visible profile. This error can be overcome in piles of particulate material using classification algorithms based on 3D range data (Thurley and Ng, 2008).

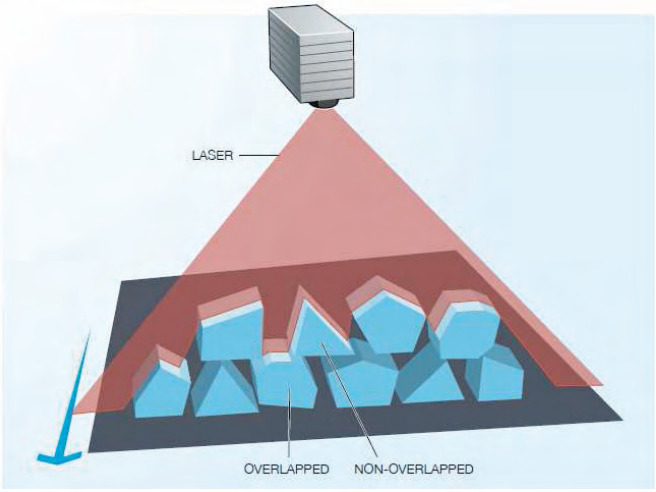

Fig. 1. Illustration of overlapped and non-overlapped particles.

Capturing error , describes the varying probability based on size, that a particle will appear on the surface of the pile. In simple terms, the larger a particle is, the more likely one is to be able to see some part of it on the surface. For example, if a single particle is as large as the height of the pile of material, then it will always be visible, whereas a very fine particle is almost certainly not visible. Thurley (2002) has explored capturing error in laboratory rock piles but it remains a source of error in this application.

Profile error, describes the fact that only one side (a profile) of an entirely visible particle can be seen making

if difficult to estimate the particles size. However, if the particle is not overlapped, best-fit-rectangle (Wang, 2006) has been demonstrated as a suitable feature for size classification based on the visible profile, that correlates to sieve size.

In addition to these errors, we note that size measurement using imaging identifies how many particles are observed of various size classes, but manual sieving measures the weight of particles in each size class. Therefore it is necessary to have a method of mapping from numbers of particles to weight of particles in order to provide a measurement of size that industry understands and can use. A technique based on physical sampling and sieving results is used in this work and explained in detail subsequently.

Particle size measurement using vision has been the subject of research and development for over 25 years (Carlsson and Nyberg, 1983) with a legacy of predominantly photographic based systems with widely varying degrees of success and no general solution available on the market.

Photographic based 2D imaging systems are subject to bias due to uneven lighting conditions, excessive shadowing, color and texture variation in the material, and lack of distinction between overlapped and non-overlapped fragments.

In their review of a commercial photographic based 2D system Potts and Ouchterlony (2005, pg. vi, viii) report that for their application the system erroneously assumes the resultant size distribution is unimodal and they conclude by expressing strong reservations saying 2D "imaging has a certain but limited usefulness when measuring the fragment size distribution in a muckpile or from a belt in an accurate way. It could probably detect rough tendencies in fragmentation variations, if the lighting conditions do not vary too much, and if cover glasses for camera lenses are kept clean".

There are a number of publications relating to 3D size measurement, Noy (2006, rocks), Frydendal and Jones (1998, sugar beets), Kim et al. (2003, river rock) Lee et al. (2005). However, Frydendal and Jones (1998), and the presenting author Thurley and Ng (2008) are the only publications (2D or 3D) to remove the bias resulting from overlapped particles. For conveyor belt applications Kim et al. (2003) and Lee et al. (2005) recommend installing a mechanical vibration feeder to separate rocks and prevent particle overlap. However, such an addition to the plant is typically impractical and for the examination of rocks in buckets (Thurley, 2009), there is no other option than to account for overlapped and non-overlapped fragments. Frydendal and Jones (1998) used graph theory and average region height to determine the entirely visible sugar beets but this relied on the regular shape and size of the beets. Only the presenting author has made this distinction between overlapped and non-overlapped particles using the advantages of 3D range data and in a manner that does not presume constraints on size or shape (Thurley and Ng, 2008).

We use an industrial measurement system on conveyor belt based on laser triangulation (a projected laser line and camera triangulation) collecting highly accurate 3D profiles of the laser line at about 3000 Hz. This high speed ensures we have a high density of 3D point data at a spacing between consecutive points in the direction of the belt of approximately 1 mm. The imaging system is installed at a limestone quarry on the conveyor belt used for ship loading and measures the material on the belt during loading every minute.

The computational speed of the analysis process is approximately 53 seconds on a 2 GHz Mobile Pentium 4 processing a data set of 590,000+ 3D points (2 m long section of the belt). Furthermore, multi-core CPUs effectively offer a linear increase in the rate at which data could be sampled from the conveyor and processed. Further advances in both algorithmic efficiency and hardware are both available to improve computational time for rapid automatic control applications.

2. RESEARCH BACKGROUND

The presented research builds upon a series of achievements and research developed on both laboratory rock piles and industrial application.

We have previously implemented an industrial measurement system on conveyor belt for iron ore pellets (Thurley and Andersson, 2007) using the same laser triangulation measurement technology. The high speed camera system ensures we have a high density of 3D point data at a spacing between consecutive points in the direction of the belt of approximately 0.5 mm. This high data density has at least two advantages. Firstly it allows us to detect small sliver regions or crescent-like regions of overlapped particles and ensure that they are not merged into other regions. And secondly, it has ensured that we could detect a very high resolution when it came to measuring the size of each iron ore pellet allowing a size distribution with very fine spacing of 5, 8, 9, 10, 11, 12.5, 13, 14, and 16+ mm size classes.

One of the key criteria for particle size measurement is therefore high data density as it defines the capacity to detect small overlapped particles, the lower limit on particle size that can be reliably detected, and the resolution of size classes detectable.

Another criteria is the computational speed of the analysis. It is generally desirable in a conveyor belt situation to sample as frequently as possible, but a sufficient sampling rate depends on the specific application. In the presented application for limestone both the lower limit of particle size (about 10 mm) and the response time to deviations in size during ship loading (about 5 minutes) are well within the computational speed and resolution capabilities of the system.

In addition we have performed a demonstration project for size measurement of rocks in underground LHD excavator buckets Thurley (2009). A 3D vision system based on laser scanners was installed on the tunnel roof in a production area of an underground iron ore mine with 3D surface data of the bucket contents being collected as the LHD unit passes beneath. The project successfully demonstrated fragmentation measurement of the rocks in the bucket, identifying overlapped rocks, non-overlapped rocks, areas of fine material, estimating the sieve size of the visible

rocks only, and the calculating the proportion of the surface that was identified as fine particles below the observable resolution of the laser scanner.

3. ANALYSIS OF 3D RANGE DATA

3.1 Segmentation

The first step is to perform the detailed image segmentation to identify the individual rock fragments. These techniques have been applied to laboratory rock piles (Thurley and Ng, 2005) and in an industrial pellet measurement system (Thurley and Andersson, 2007) and were adapted to this application. The technique is predominantly based on morphological image processing, based largely on various edge detection techniques to facilitate seed formation for the watershed segmentation algorithm.

Figure 2 shows a closeup image of rocks on the conveyor and the automated segmentation result.

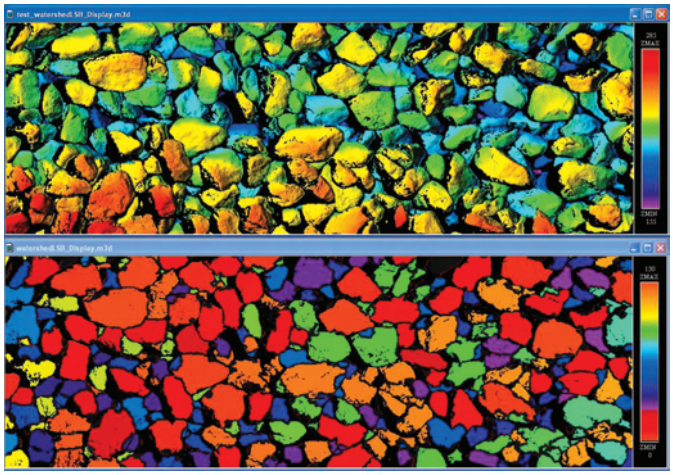

Fig. 2. Rocks on conveyor and automated segmentation for limestone aggregate, 40–70 mm size range.

3.2 Non-overlapped Particles

In order to explain the determination of overlapped and non-overlapped particles it is necessary to introduce a boundary following algorithm developed by Thurley and Ng (2008) for the purpose of overlapped particle detection.

The algorithm begins with a segmentation of a pile of particulate material and examines each region in the segmentation. For each region in the segmentation we identify a series of prominent points equally spaced around the perimeter of the region.

Looking at figure 3 we see a representation of two regions (one overlapping the other) with a series of prominent points marked for region R_i.

We then use these points to define small local areas in which we examine the height of the regions in that local area. In the magnified section of figure 3 you can see a circular area about point g, we examine this area, denoted N_g and calculate the average height of all of the points in the region R_i that intersect area N_g, and we calculate the average height of all of the points in the

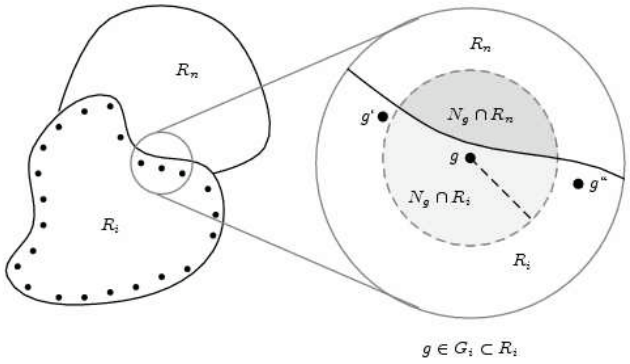

Fig. 3. Boundary following algorithm

region R_n that intersect region N_g. By comparing these two average height values we can evaluate whether in the local neighbourhood of point g, region R_i is either above or below region R_n.

This determination is used to determine overlapped/non-overlapped particles by counting the ratio of points g where region R_i is above region R_n.

This distinction allows us to eliminate misclassification of overlapped rocks are if they were smaller non-overlapped rocks.

We apply an equivalent strategy to that applied on laboratory rock piles (Thurley and Ng, 2008) using the visibility ratio and selecting a decision boundary of 0.65. Figure 4 shows only the rocks that were classified as non-overlapped from figure 2.

We will perform sizing on the non-overlapped rocks for which we can make a confident size prediction, and we will ignore overlapped rocks.

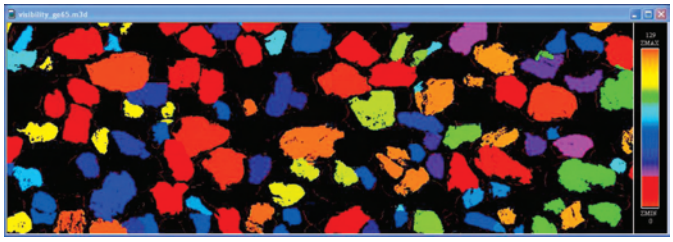

Fig. 4. Non-overlapped rocks automatically identified from figure 2, 40–70 mm size range.

3.3 Sizing

Sizing begins by calculating a feature called best-fit-rectangle area for each of the regions identified as non-overlapped fragments from the segmentation (figure4). The best-fit-rectangle is the rectangle of minimum area that fits around the 2D projection of each region. We ignore the height component of the points in a region and calculate an arbitrarily rotated best-fit-rectangle. We have used this feature previously (Thurley and Ng, 2008; Thurley and Andersson, 2007, laboratory rock piles, iron ore pellets) and demonstrated its suitability for estimating sieve size of non-overlapped particles.

In order to classify best-fit-rectangle areas into sieve size classes however, we require a series of decision boundaries.

In effect, thresholds that define which area values separate one size class from another. To determine these values we use some sieving data that corresponds to some of our image analysis results.

During the measurement campaign we collected a 3D data set of the surface of the rock stream every minute for approximately 13 hours of production. In this time we obtained just over 600 3D data measurement sets of limestone on the conveyor belt, and automatically identified and sized over 140,000 rocks. In addition, the mining company obtained some manual samples from the conveyor using a automated sampler, and subsequently sieved these in the laboratory. Table 1 shows these sieve results. What we see is that two distinct product ranges of material were being loaded at different times. Firstly the 40–70 mm product, then the 20–40 mm product, before changing back to the 40–70 mm. For a given sieving, most of the material is within the product size range, but there is always some small proportion above and below this range. We also note that the sieve decks were changed between the two different products.

Table 1. Sieving results (cumulative %)

		Product				
Sieve	40-70mm	20–40 mm			40–70 mm	
Size		Sieving Time				
(mm)	21:20	23:05	00:15	06:50	09:45	11:40
> 75	100	100	100	100	100	100
< 75	100	100	100	100	95.2	89.9
< 63	77.8	100	100	76.2	78.1	59.6
< 50	45.9	100	100	40.8	40.9	28.1
< 45	–	98.7	100	–	–	–
< 40	5.83	87.1	86.8	6.56	4.79	3.65
< 37.5	2.43	–	–	2.82	1.86	1.57
< 31	–	44.2	36.3	–	–	–
< 25	0	14.6	10.6	0	0	0
12–20	0	0.736	0.762	0	0	0

We select two data sets from each product range (times 23:05, 00:15, 09:45, and 11:40) and use the sieving data and corresponding image analysis results to calculate decision boundaries for mapping best-fit-rectangle area into sieve size class.

We use the Nelder and Mead (1965) iterative error minimisation process to calculate decision boundaries with minimised error. This optimisation method is available both in Matlab using function `fminsearch`, or in the statistical package R using function `optim` which we use here. Given an initial estimate of the decision boundaries we use Nelder-Mead minimisation to produce a final set of boundaries.

The Nelder-Mead optimisation takes an estimate of the decision boundaries and calculates the error at that estimate (we define this error function in more detail in the next section). The optimisation modifies the decision boundaries slightly following a range of internal rules before repeating the process. Changes that reduce the error are kept, while changes that increase the error are typically discarded. We first calculate optimum decision boundaries for each set of sieving data and then calculate the median values as the initial estimates for the Nelder-Mead and generate the error minimised result.

Figure 5 shows the distribution of best-fit-rectangle (BFR) area measurements for the non-overlapped rocks calculated by the system for the two different products from all 600+ 3D measurements. We can clearly see that when the smaller product is on the belt, smaller values of the BFR area are generally calculated. We also show the location of the decision boundaries for each sieve size on the bottom axis as calculated using the Nelder-Mead optimisation.

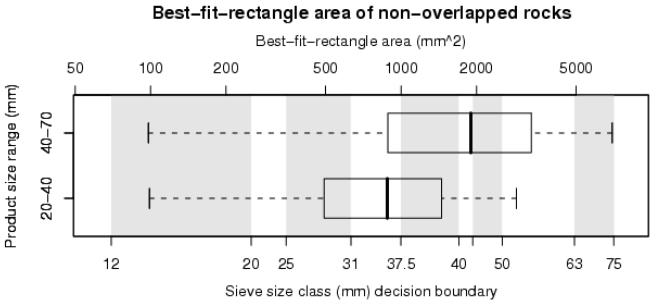

Fig. 5. Best-fit-rectangle areas results for the Non-overlapped rocks by product size range.

3.4 Mapping from Number to Weight

One of the complications for image analysis systems is that they can measure the number of observable particles, and using classification strategies for size can calculate number of particles in each size class. However, what is required is the estimated weight of the material in each size class as this percentage by weight is what is measured by sieving and required by industry. Therefore it is necessary to convert number of particles by size class into an estimated weight by size class. We do this by collecting sieving results and counting the number of particles in each size class in order to determine an average weight of a fragment by size class as shown in table 2.

Table 2. Mean Particle Weight by Size Class

Sieve	Mid	Mean Particle Weight (g)					
Size	Size	Time of Sieving					
(mm)	(mm)	21:20	23:05	0:15	6:50	9:45	11:40
> 75	80	–	–	–	–	793	719
63–75	69	540	–	–	480	504	509
50–63	56.5	289	–	–	276	285	311
45–50	47.5	na	168	–	na	na	na
40–50	45	164	na	na	172	172	187
40–45	42.5	na	115	117	na	na	na
37.5–40	38.8	132	na	na	129	105	148
31–40	35.5	na	73.7	72.3	na	na	na
31–37.5	34.3	na	na	na	na	na	na
25–37.5	31.3	72.5	na	na	80.2	84.3	99.9
25–31	28	na	42.3	44.0	na	na	na
20–25	22.5	–	27.1	27.6	–	–	–
12–20	16	–	9.21	7.98	–	–	–

The immediate thing that one notes from table 2 is that different arrangements of sieve decks were used at different times (for the different products) complicating the capacity to compare and combine the results. As a result we calculate a polynomial of best-fit for the sieve mid-size versus weight. This provides a continuous and consistent estimate of weight for any given size class that we wish to estimate with the imaging.

Based on the data in table 2 we calculate a third order polynomial where x is the mid size of the sieve range and the weight is given by $f(x) = 0.001208x^3 + 0.01494x^2 +$

$0.5306x$ with correlation $R^2 = 0.9909$. The graph of table 2 and the best-fit polynomial is not shown due to page limitations.

This mismatch between measuring numbers of particles and correlating against weight affects the Nelder-Mead error minimisation process. As a result we use the weights calculated using the best-fit polynomial within the Nelder-Mead error minimisation. We express this error function as a sum of squares as shown in equation (1). The function uses a normalized weight value derived from the polynomial weight function f. The normalized weight provides a weight of 1 for the heaviest size class at a given time t, with the lighter weights scaled relatively to this value. The purpose of this normalization is to ensure that heavier product ranges do not dominate the error function. Without this normalization the results for the 40-70mm product dominate the optimization effectively ignoring the error for the 20-40mm product.

$$\epsilon = \sum_{t} \left[\sum_{i=1}^{N} \left[(C_{x,t} - S_{x,t})\, \widehat{W}_{x,t} \right]^2 \right] \qquad (1)$$

$$\widehat{W}_{x,t} = \frac{f(x)}{max_t(f)}$$

t	Time of day
x	Sieve size class
N	Number of sieve size classes
$C_{x,t}$	Calculated value of the size class x at time t
$S_{x,t}$	Sieving result for size class x at time t
$f(x)$	Weight of size class x using polynomial weight function
$max_t(f)$	Weight of heaviest size class at time t
$\widehat{W}_{x,t}$	Normalized weight

Furthemore, as decision boundaries must be monotonically increasing with size class x (the larger the size class the larger the decision boundary), we must further constrain the error-function by using a penalization factor when the decision boundaries are out of order. Specifically we scale the error by the amount that any consequtive decision boundaries is out of order. Without this constraint the error minimization can generate meaningless out of order results.

Using the optimised Nelder-Mead decision boundaries for determining the sieve size class boundaries (depicted in figure 5) we produce estimates of the sieve size distributions for the 606 measurement sets. The results are presented in figure 6 with the sieve data from table 1 overlayed as colored points.

If we look only at the sieving results from 0:15 and 6:50, and the two imaging mesurements that correspond to these times we can plot a typical log-linear cumulative size distribution curve as shown in figure 7.

4. DISCUSSION

The imaging results (figure 6) are shown to clearly trend in the right direction tracking changes in the material size. Furthermore, in the higher size classes, 50, 63, 75, where decision boundaries could be set for the 40–70 mm product independantly of the 20–40 mm product, the imaging results appear to track the sieving results well.

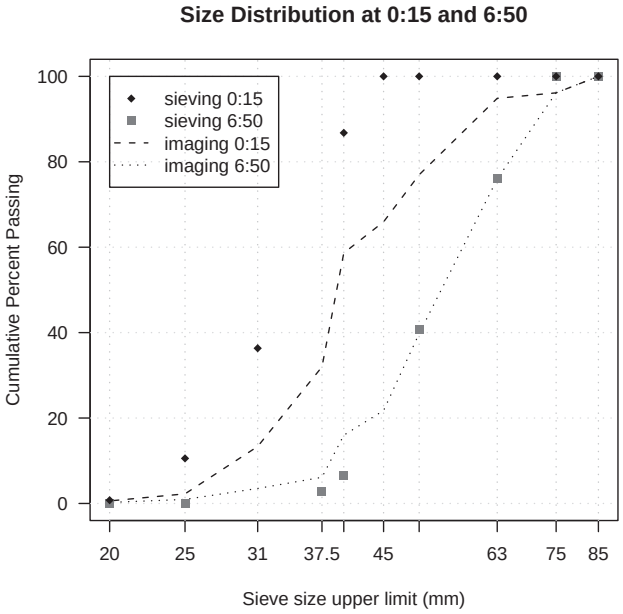

Fig. 7. Imaging and sieving results for 2 measurements and sieve results at 0:15 and 6:50.

If we examine figure 6 and compare it to the cumulative sieving results in table 1 we can see that the image analysis overestimates the amount of < 40 mm size class in the 40–70 mm product, by about 10%, and underestimates the cumulative amount in the 20–40 mm product by about 25%.

The key problem is that an average weight by size class will work fine if the fragments are always uniformly distributed across that size class. The polynomial weight function attempts to produce a reasonable average weight by size class for all cases but further work is necessary to understand this relationship.

Improvements are expected after performing additional sieving experiments with a much finer sieving, using consistent decks for all products, such as 0, 12, 20, 25, 31, 37, 40, 45, 50, 63, 75 etc. instead of changing the decks as was done here. This sort of high resolution sieving will be carried out in an upcoming measurement and sieving trial to collect the necessary field measurements so that we can more accurately represent fragment weight variatios by size class.

ACKNOWLEDGEMENTS

Thank you to ProcessIT Innovations for their continuing support in developing and intiating industry projects. Thank you to the MinBaS II research program and Nordkalk for their participation and support, and a thank you to our meaurement technology partners, MBV-Systems.

REFERENCES

Carlsson, O. and Nyberg, L. (1983). A method for estimation of fragmentation size distribution with automatic image processing. In *Proceedings of the First International Symposium on Rock Fragmentation by Blasting – FRAGBLAST*, 333–345. Luleå, Sweden.

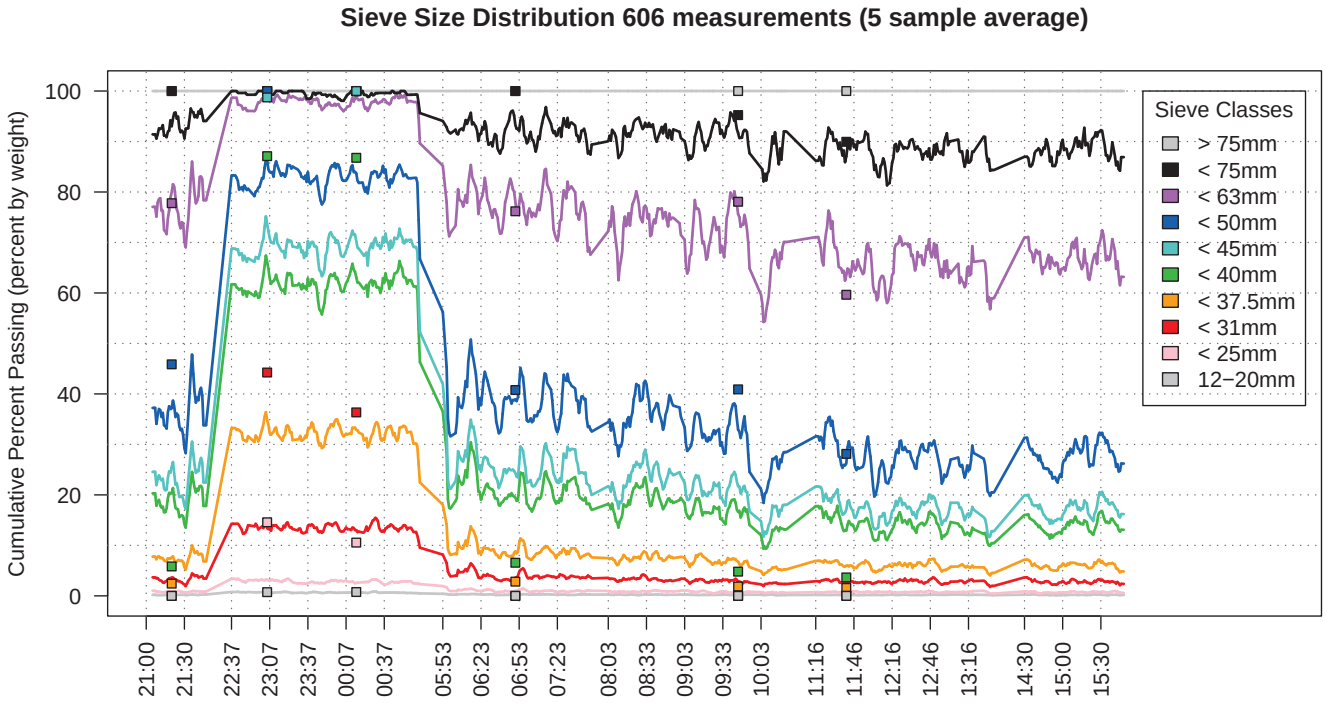

Fig. 6. Imaging and sieving results for 606 measurements over 10 hours of loading.

Chavez, R., Cheimanoff, N., and Schleifer, J. (1996). Sampling problems during grain size distribution measurements. In *Proceedings of the Fifth International Symposium on Rock Fragmentation by Blasting – FRAGBLAST 5*, 245–252. Montreal, Quebec, Canada.

Frydendal, I. and Jones, R. (1998). Segmentation of sugar beets using image and graph processing. In *ICPR 98 Proceedings – 14th International Conference on Pattern Recognition*, volume II, 16–20. Brisbane, Australia.

Kim, H., Haas, C., Rauch, A., and Browne, C. (2003). 3d image segmentation of aggregates from laser profiling. *Computer Aided Civil and Infrastructure Engineering*, 254–263.

Lee, J., Smith, M., Smith, L., and Midha, P. (2005). A mathematical morphology approach to image based 3d particle shape analysis. In *Machine Vision and Applications*, volume 16(5), 282–288. Springer–Verlag.

Nelder, J. and Mead, R. (1965). A simplex method for function minimisation. *The Computer Journal*, 7, 308–313.

Noy, M.J. (2006). The latest in on-line fragmentation measurement - stereo imaging over a conveyor. In *Proceedings of the Eighth International Symposium on Rock Fragmentation by Blasting – FRAGBLAST 8*, 61–66.

Potts, G. and Ouchterlony, F. (2005). The capacity of image analysis to measure fragmentation, an evaluation using split desktop. Technical report, Swebrec - Swedish Rock Breaking Institute. ISSSN 1653-5006.

R Project (2005). *R: A language and environment for statistical computing*. R Foundation for Statistical Computing, Vienna, Austria. URL `http://www.R-project.org`. ISBN 3-900051-07-0.

Rosato, A., Strandburg, K., Prinz, F., and Swendsen, R. (1987). Why the brazil nuts are on top: Size segregation of particulate matter by shaking. *Physical Review Letters*, 58(10).

Thurley, M.J. (2002). *Three Dimensional Data Analysis for the Separation and Sizing of Rock Piles in Mining*. Ph.D. thesis, Monash University. URL `http://image3d6.eng.monash.edu.au/thesis.html`.

Thurley, M.J. (2009). Fragmentation size measurement using 3d surface imaging. In *Proceedings of the Ninth International Symposium on Rock Fragmentation by Blasting – FRAGBLAST 9*. In submission.

Thurley, M. and Andersson, T. (2007). An industrial 3d vision system for size measurement of iron ore green pellets using morphological image segmentation. *Minerals Engineering*, 21(5), 405–415. URL `http://dx.doi.org/10.1016/j.mineng.2007.10.020`.

Thurley, M. and Ng, K. (2005). Identifying, visualizing, and comparing regions in irregularly spaced 3d surface data. *Computer Vision and Image Understanding*, 98(2), 239–270. URL `http://dx.doi.org/10.1016/j.cviu.2003.12.002`.

Thurley, M. and Ng, K. (2008). Identification and sizing of the entirely visible rocks from segmented 3d surface data of laboratory rock piles. *Computer Vision and Image Understanding*, 111(2), 170–178. URL `http://dx.doi.org/10.1016/j.cviu.2007.09.009`.

Wang, W. (2006). Image analysis of particles by modified ferret method – best-fit rectangle. *Power Technology*, 1–10.

Fragmentation Size Measurement using 3D Surface Imaging

M. J. Thurley
Luleå University of Technology, Luleå, Sweden

ABSTRACT: Advances in developing vision systems for fully automated, non-invasive, rapid particle sizing in the mining and aggregates industries are presented using the example of fragmentation measurement of ore in an underground LHD unit bucket. 3D surface data of the bucket contents was collected during operation and fully automated offline processing of the data was performed on 424 data sets, determining the individual fragments in the bucket and estimating their sieve size. Results are presented covering; fully automatic fragment identification, determination of non-overlapped and overlapped fragments to eliminate misclassification of overlapped fragments as smaller fragments, automatic identification of areas of fine material below the resolution of the 3D sensor, and sizing based on the measured 3D fragment profile that takes fragment overlap into consideration. The presented research allows the possibility of feedback to blasting, and automatic control of crushers when applied to conveyor belt applications.

1 INTRODUCTION

In the mining and aggregates industries a great deal of effort goes into measuring or estimating the size distribution of particulate material. One of the reasons is that suppliers of aggregate material are paid to supply a specific size range of material. For both industries there is also a fundamental question about process control & optimization such as in crushers and for processing plants that want to control their value-added products such as iron ore pellets.

Furthermore, blasting and caving are very cost effective methods of rock breakage, but they are not processes that are easily quantified. Mine and quarry operators want to measure the fragmentation results of these activities but sieving is impractical as a routine assessment tool.

Sampling and sieving is routinely used by both industries to evaluate particle size in their processing plants but it is intermittent, invasive, slow and not suited to process feedback or timely measurement of quality control.

As a result there is an opportunity for online, noncontact, automated machine vision systems for measurement of particle size on conveyor, in buckets (such as the excavator shown in Figure 1), or in

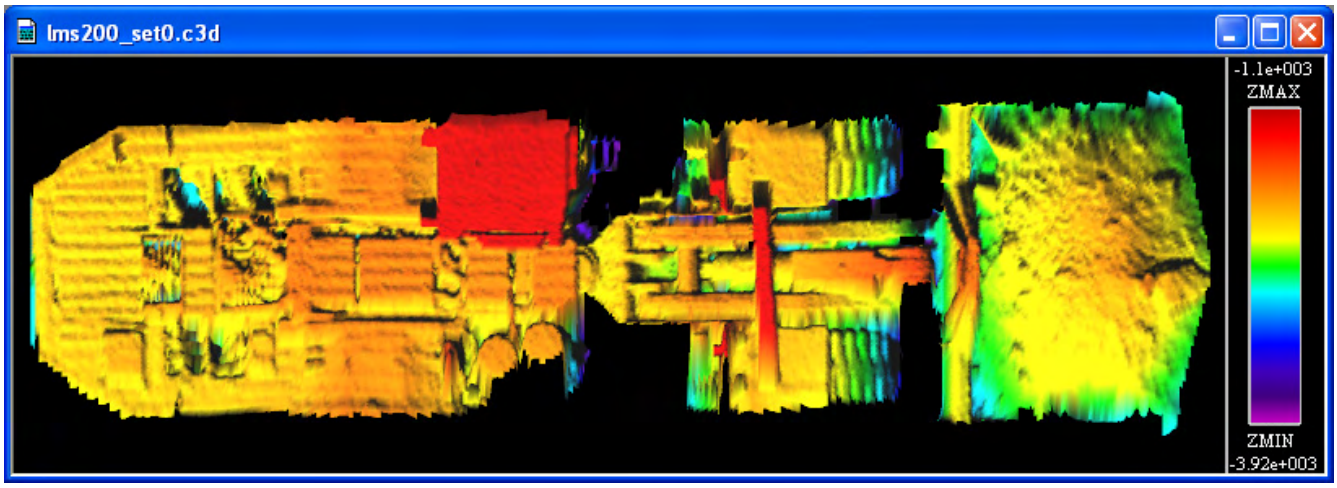

Figure 1. 3D surface data of a Toro2500E LHD unit.

static piles, that can provide the necessary accuracy and fast feedback.

Particle size measurement using vision has been the subject of research and development for over 25 years (Carlsson & Nyberg 1983) with a legacy of predominantly photographic based systems with widely varying degrees of success.

Photographic based 2D imaging systems are subject to bias due to uneven lighting conditions, excessive shadowing, color and texture variation in the material, perspective distortion, and lack of distinction between overlapped and non-overlapped particles.

In their review of a commercial photographic based 2D system Potts & Ouchterlony (2005, pg. vi, viii) report that the system erroneously assumes the resultant size distribution is unimodal and they conclude by expressing strong reservations saying 2D "imaging has a certain but limited usefulness when measuring the fragment size distribution in a muckpile or from a belt in an accurate way. It could probably detect rough tendencies in fragmentation variations, if the lighting conditions do not vary too much, and if cover glasses for camera lenses are kept clean".

There are a number of publications relating to 3D size measurement, Noy (2006, rocks), Frydendal & Jones (1998, sugar beets), Kim et al. (2003, river rock), Lee et al. (2005), and the presenting author (Thurley & Andersson 2007). However, Frydendal & Jones (1998) and the presenting author (Thurley & Ng, 2008), are the only publications (2D or 3D) to remove the bias resulting from overlapped particles. For conveyor belt applications Kim et al. (2003) and Lee et al. (2005) recommend installing a mechanical vibration feeder to separate rocks and prevent particle overlap. However, such an addition to the plant is typically impractical and for the examination of rocks in buckets, there is no other option than to account for overlapped and non-overlapped fragments. Frydendal & Jones (1998) used graph theory and average region height to determine the entirely visible sugar beets but this relied on the regular shape and size of the beets. Only the presenting author has made this distinction between overlapped and non-overlapped particles using the advantages of 3D surface data and in a manner that does not presume constraints on size or shape (Thurley & Ng 2008, laboratory rock piles).

Regarding the detection of fines, Noy (2006) states that their algorithm can distinguish fines and supporting images are shown, but specific details of the algorithm are not provided.

The research presented here details a two feature classifier that allows for the detection and exclusion of areas of fines.

2 RESEARCH BACKGROUND

The presented research builds upon a series of achievements and research developed both in the laboratory and in industrial applications.

We have previously implemented an industrial measurement system on conveyor belt for iron ore pellets (Thurley & Andersson 2007) using laser triangulation collecting highly accurate 3D profiles of the laser line at about 4000Hz. This ensures we have a high density of 3D point data at a spacing between consecutive points in the direction of the belt of approximately 0.5mm. This high data density has at least two advantages. Firstly it allows us to detect small sliver regions or crescent-like regions of overlapped particles and ensure that they are not merged into other regions. And secondly, it has ensured that we could detect a very high resolution when it came to measuring the size of each iron ore pellet allowing a size distribution with very fine spacing of 5, 8, 9, 10, 11, 12.5, 13, 14, and 16+mm size classes.

One of the key criteria for particle size measurement is therefore high data density as it defines the capacity to detect small overlapped particles, the lower limit on particle size that can be reliably detected, and the resolution of size classes detectable.

Another criterion is the computational speed of the analysis. It is generally desirable in a conveyor belt situation to sample as frequently as possible, but a sufficient sampling rate depends on the specific application. Computational speed is significantly improved if the data is regularly spaced along the x and y axes.

The computational speed of the analysis process outlined in the pellet system (Thurley & Andersson 2007) has now been improved to 35 seconds on a 2GHz Mobile Pentium 4 processing a data set of 500,000+ 3D points with effectively linear speed improvements available through multi-core CPUs.

Our research is focused on the analysis of 3D surface data and not the hardware technology used to collect the 3D data. Whether that data comes from laser triangulation, laser range finders, or stereo photogrammetry is not overly important to the analysis. The primary considerations for choosing a given hardware solution is suitability for a given application.

3 BUCKET MEASUREMENT

We report on the results of a demonstration project for the sizing of rock material in the bucket of an underground LHD excavator

The demonstration project had three broad aims as follows;

1 To demonstrate the potential to collect 3D data of the LHD bucket without any interruption or interference with the LHD unit.

2 To perform fragmentation size measurement.
3 To perform volume measurement of the bucket contents (this objective is not detailed in this paper).

The objective for the mining company is to obtain size distribution information to provide feedback to the underground blasting, a process for which they currently have no reliable size measurement and for which sieving is completely impractical.

The LHD unit digs out a load of rocks from the drawpoint of the blast, drives through the tunnels to a dumping shaft, and then returns to repeat the process every 2–4 minutes.

The data capture requires an alternative sensor as the geometry of the vehicle and tunnel is too large for the laser triangulation hardware used in the pellet system. Data collection was achieved using a hybrid system based on two sensors. Firstly, a SICK LMS200 scanning laser range finder to continuously scan, providing the data for detecting the LHD unit and calculating the bucket volume, and additionally, a SICK LMS400 scanning laser range finder to provide the high resolution data necessary for fragmentation measurement, scanning only when the LHD unit is detected. The scanners are roof mounted, looking down, and measure height values as it scans across the vehicle. The third dimension is parallel to the motion of the vehicle and can be calculated based on the time taken to collect the data and the speed of the vehicle. However, the speed of the vehicle is not known and will be estimated based on detecting the bucket in the data which is of known length.

One of the most critical requirements of the sensor is data density as this impacts the capacity to detect overlapped particles and the accuracy with which sizing can be estimated. Therefore, the capacity to collect a lot of data is more important than the height accuracy. We operated the LMS400 scanner at 290Hz with a 0.2 degree step angle capturing 3D data points with a spacing of approximately 10mm with a range error of approximately ±5mm. Vehicle speed in the production level was 2 to 3m/s.

The expected material size will be 0–1000mm with sizes below 100mm not being required to be measured. Material below 100mm also constitutes fines in this case as it is below the expected detection limit of the vision system.

We now state the specific sizing objectives of the demonstration project;

- Fully automated offline sizing of 200 or more LHD buckets.
- Rocks classified into size classes, 100, 200, 300, 400, 500, and 600+mm.
- Sizing of all visible fragments.

4 ANALYSIS

1 In order to achieve the project objectives the following tasks were performed;
2 Collect 3D data of each LHD bucket.
3 Identify the bucket.
4 Preprocess the 3D data to remove noise.
5 Segment the 3D data of the LHD bucket to identify individual fragments.
6 Identify areas of fines versus rock fragments.
7 Identify which rocks are overlapped and which are non-overlapped.
8 Sizing.

4.1 *Identify the bucket*

The spacing between data points in the direction of motion of the LHD (the y axis) is first assigned at a constant value based on the known length of the LHD. This estimate can be quite erroneous as we observed cases where acceleration produced a bucket scaling error of +16% and -27% which would directly translate into sizing and volume measurement error. Therefore, we detect the location of the bucket in the 3D data and rescale the y axis so that the data matches the known length of the bucket. The bucket is approximately 2.93m in length when in fixed position for driving as calculated from the Toro2500E schematic from Sandvik. To identify the bucket we calculate the front and back of the bucket by analyzing a graph of number of data points measured on the bucket per laser scanline.
Figure 2 shows a reflectance image taken by the laser scanner with noted scanline numbers and Figure 3 the corresponding graph of 3D points per scanline with the automatically detected front and back of the bucket.

The front of the bucket is always after a series of zero values in the Figure 3 graph and is quickly followed by a steep increase to a maximal value of 300+, and the back is always a large negative gradient down from this maximal value. Figure 4 shows the 3D data of the bucket after it has been scaled correctly based on this bucket detection algorithm.

4.2 *Preprocessing*

In this stage we remove noise using a simple 8 neighbor median filter, followed by removal of points that had no immediate neighbors. Large noise values tend to occur at the edges of the bucket, where partial reflection of the laser spot can occur. The combination of these filters was sufficient to remove observable noise.

After noise removal the data is resampled to a regular grid in the x, y plane to greatly improved computational efficiency. In this case computation time for the entire sizing process of under 10 seconds on a 2GHz Mobile Pentium 4.

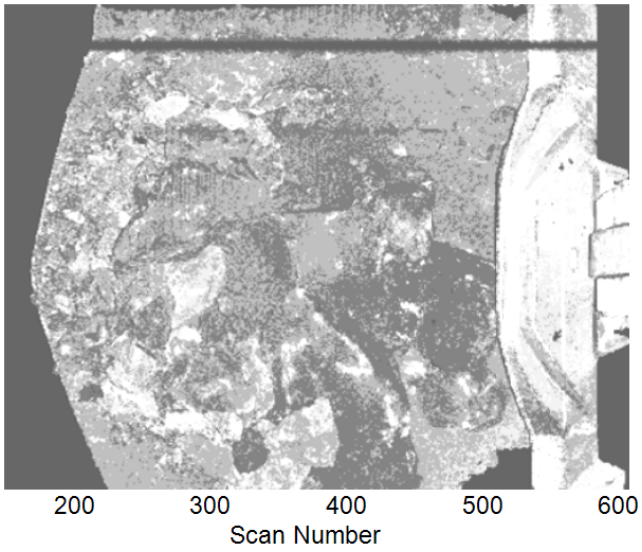

Figure 2. Image of each scanline of the LMS400 laser scanner.

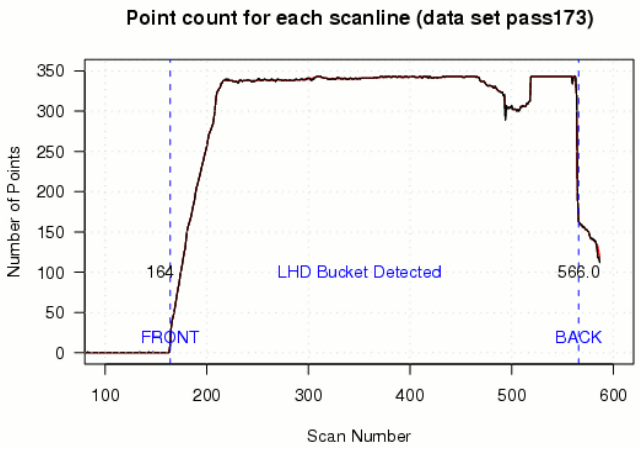

Figure 3. Number of 3D data points by scan number.

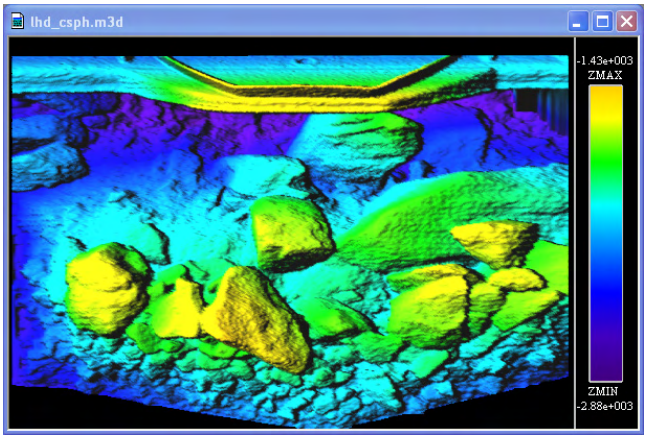

Figure 4. LHD bucket 3D data, correctly scaled.

4.3 *Segmentation to identify fragments*

The first stage of the image segmentation phase is to find the area of rocks in the bucket, versus the visible metal parts of the bucket. A well known segmentation algorithm called *watershed segmentation* using two seeds is used to find two regions, the bucket which must intersect the back of the data, and the rocks, which intersects the middle of the data.
Figure 5 shows the result of this segmentation and clearly identifies the bucket. The bucket is then removed allowing further processing to identify the individual rock fragments.

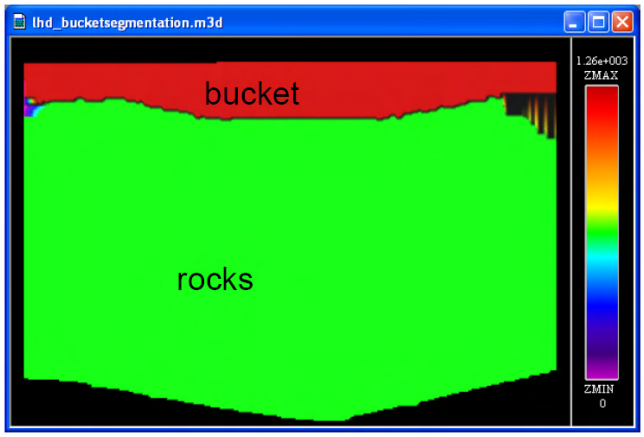

Figure 5. Segmentation to identify the metal portion of the bucket versus the rocks.

The next step is to perform the detailed image segmentation to identify the individual rock fragments. These techniques have been applied to laboratory rock piles (Thurley & Ng 2005) and in an industrial pellet measurement system (Thurley & Andersson 2007) and were easily adapted to this application. The technique is predominantly based on morphological image processing, based largely on various edge detection techniques to facilitate seed formation, followed by the watershed segmentation algorithm.

The significant difference in this application is the presence of fines. Fines create a significant portion of the pile surface where the laser scanner cannot ‘see’ individual particles, but only a noisy, but relatively smoothly varying surface. At this stage of the segmentation somewhat randomly shaped regions are identified where there are areas of fines. Figure 12 shows the automated segmentation corresponding to Figure 4 with Figure 8 and Figure 9 showing another data set with its corresponding segmentation.

4.4 *Boundary following algorithm*

In order to explain the following two sections on identifying areas of fines and distinguishing between overlapped and non-overlapped particles it is necessary to introduce a boundary following algorithm developed by Thurley & Ng (2008) for the purpose of overlapped particle detection.

The algorithm begins with a segmentation of a pile of particulate material and examines each region in the segmentation. For each region in the segmentation we identify a series of prominent points equally spaced around the perimeter of the region.

Looking at Figure 6 we see a representation of two regions (one overlapping the other) with a series of prominent points marked for region R_i. We then use these points to define small local areas in which we examine the height of the regions in that local area. In the magnified section of Figure 6 you can see a circular area about point g, we examine this area, denoted N_g and calculate the average height of all of the points in the region R_i that intersect area N_g, and we calculate the average height of all of the points in the region R_n that intersect region N_g. By comparing these two average height values we can evaluate whether in the local neighborhood of point g, region R_i is either above or below region R_n.

This determination will be used both to determine areas of fines, and overlapped/non-overlapped particles. For the height measure used to detect fines, we sum the absolute value of this height difference for all the points around the perimeter. For the visibility ratio used to distinguish overlapped/non-overlapped particles, we count the ratio of points g where region R_i is above region R_n.

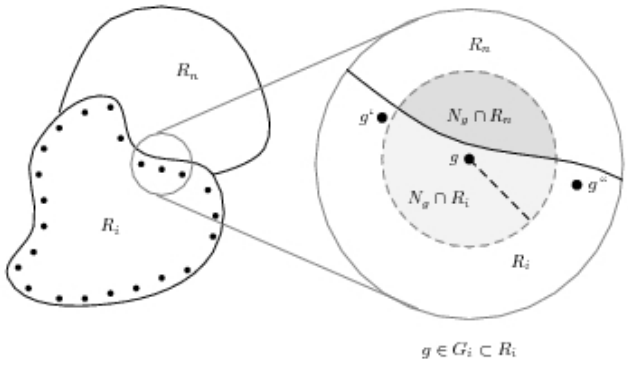

Figure 6. Boundary following algorithm.

4.5 *Identify Areas of Fines*

A new algorithm has been developed that identifies which regions in the segmentation correspond to areas of fines, and which to rocks. It is based on the observation that areas of fines are relatively smoothly varying surfaces compared to rock surfaces which are very abruptly changing at the edges. The algorithm examines the degree to which the height of the range data changes around the boundary of the identified regions in the segmentation.

Both the height measure and visibility ratio introduced above are used in the classification of areas of fines. If we consider the bucket data set in Figure 8 and Figure 9 we can see that there are a lot of regions that are areas of fines. By manually classifying each region in this data set we create a "truth" data set upon which we will create an automatic classifier. We manually classified each region in this data set as either; rock, area of fines, unknown, many-rocks (an under-segmentation) or rock-pieces (an over-segmentation). Then for each region we calculate the height measure and visibility ratio. Figure 7 shows the plot of these results with the height measure along the horizontal axis, and the visibility ratio along the vertical axis. What you can immediately see, is that the regions that were manually identified as fines (as denoted by red + symbols) are towards the left and bottom of the graph, and regions that were manually identified as rocks (denoted by black o symbols) appear more towards the right and top of the graph.

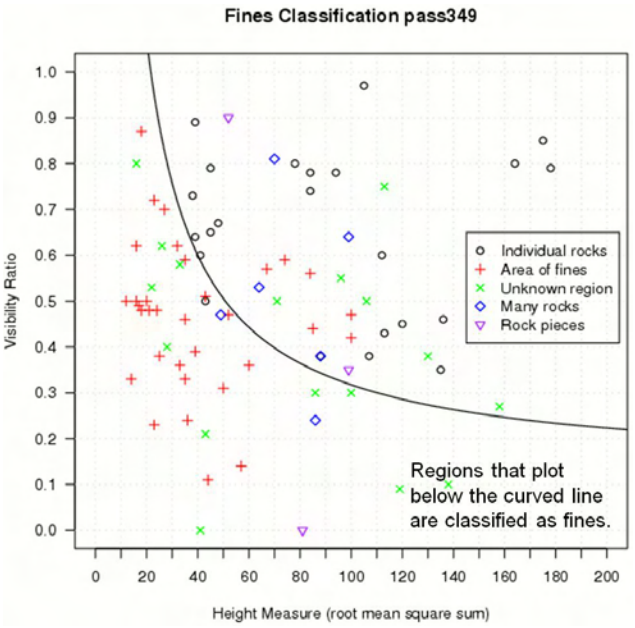

Figure 7. Fines classification graph for Figure 9.

By using this spatial relationship we can define an automatic classifier, that is, a line that separates the fines (red + symbols), and the rocks (black o symbols) as shown by the curved line in the graph. When we process a different data set we will calculate the visibility ratio, and the height measure for each region, and determine if that region would plot beneath the line. If so, that region will be classified as an area of fines.

No classification strategy is perfect but most regions are classified correctly. For Figure 7, 21 of the 22 rock regions are classified correctly, and 27 of the 33 fines regions are classified correctly with the results shown in Figure 10. When we apply the classifier to our first data set we get the results shown in Figure 13.

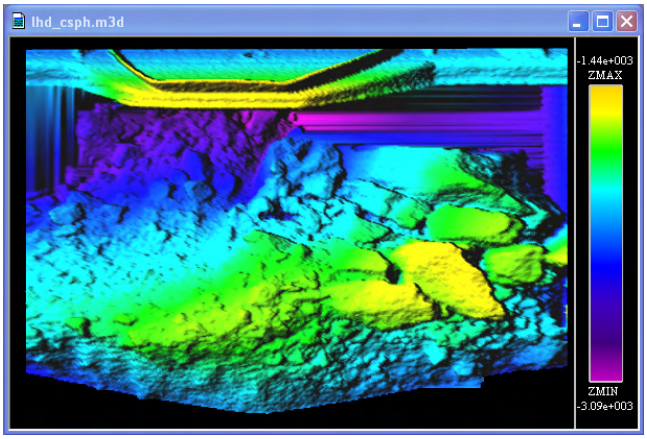

Figure 8. LHD bucket 3D data, second set.

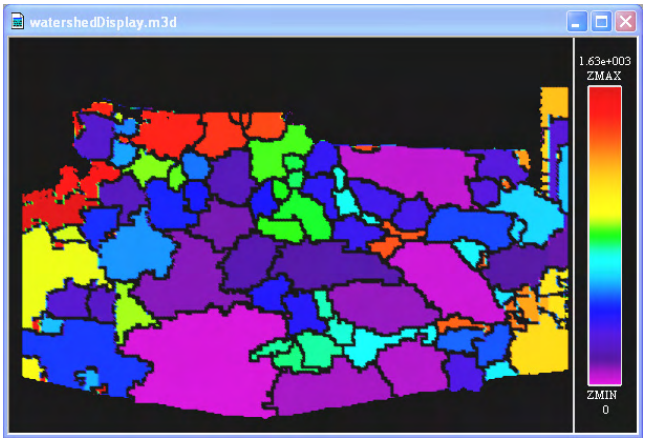

Figure 9. Automated segmentation for Figure 8.

Figure 10. Automated segmentation with fines removed from Figure 9.

4.6 *Identify overlapped & non-overlapped fragments*

At this stage we examine the regions identified as rock fragments and use a proven classification strategy (Thurley & Ng 2008; Thurley & Andersson 2007) to determine which rocks are significantly non-overlapped, and can therefore be accurately sized based on their visible profile, and which rocks are overlapped.

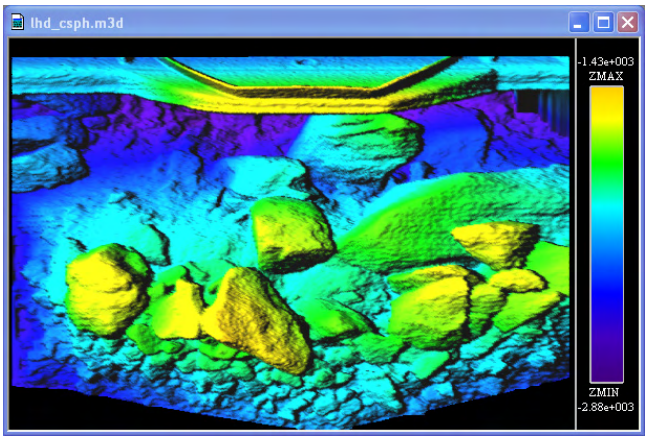

Figure 11. LHD bucket 3D data, first set.

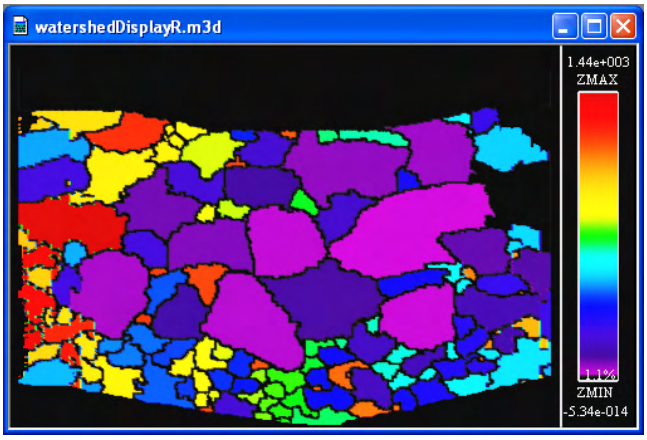

Figure 12. Automated segmentation for Figure 11.

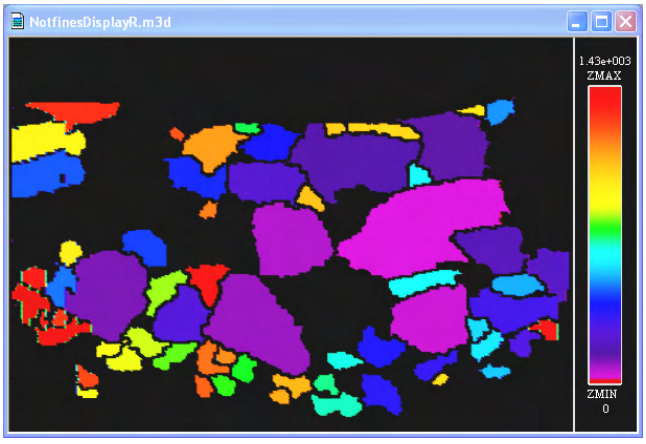

Figure 13. Automated segmentation with fines removed from Figure 12.

This distinction between overlapped and non-overlapped allows us to eliminate misclassification of overlapped rocks as if they were smaller non-overlapped rocks.

We apply an equivalent strategy to that applied on laboratory rock piles (Thurley & Ng 2008) using the visibility ratio and selecting a decision boundary of 0.7. Figure 14 shows the final classification strategy and Figure 15 shows only the rocks that were classified as non-overlapped from Figure 13.

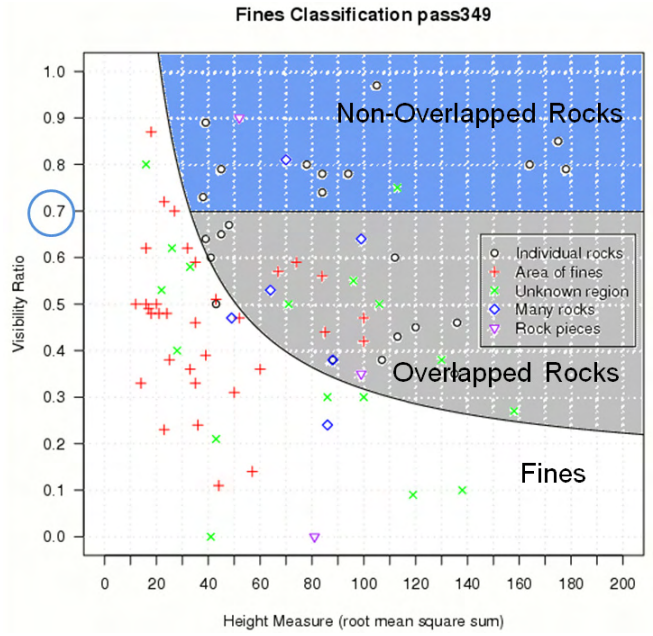

Figure 14. Overlapped particle and fines classification graph for Figure 9.

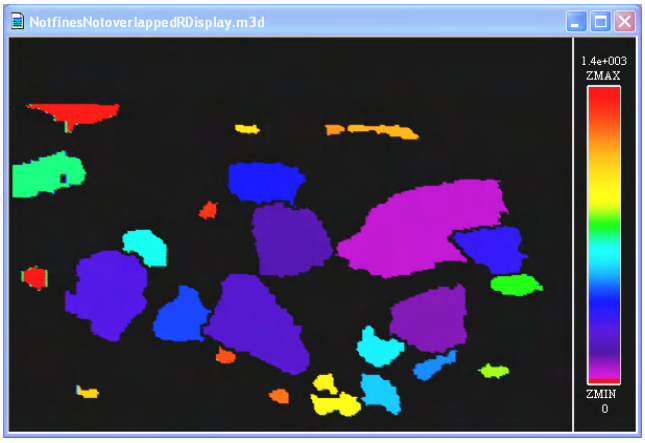

Figure 15. Automated segmentation with overlapped rocks removed and fines removed from Figure 12.

4.7 *Sizing*

Sizing is performed using a feature called best-fit-rectangle area which we have found through our work with rock and pellets correlates well to sieving, if the particle is non-overlapped. The best-fit rectangle is the encompassing rectangle of minimum area as shown in Figure 16.

In order to classify best-fit-rectangle areas into sieve size classes however, we require a series of decision boundaries. In effect, thresholds that define what area value separates one size class from another. Typically this would be calculated in the laboratory on samples of the ore relevant to the application but this was not practical both in terms of the short time frame of the demonstration project, and the large size classes, so a more generic approach had to be taken.

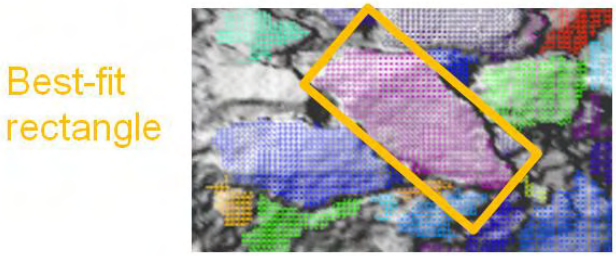

Figure 16. Example of best-fit-rectangle area.

Based on observations from the author's doctoral thesis using a sample of crushed basalt the following approach was used. If size class A is between *i* and *j*, and size class B is between *j* and *k*, then the decision boundary for the classification between A and B is the square of the mid-point of size class B, $([j+k]/2)^2 = [j+k]^2/4$ mm^2. This approach is admittedly ad-hoc and requires further investigation so that the decision boundaries can be tailored to the ore being sized as it is related to the particle shape of each size class and is material dependant. For the purposes of the demonstration project and to show proof-of-concept the approach was sufficient.

For overlapped particles we use a probabilistic sizing strategy. All we know about a given overlapped particle is that it cannot be smaller than the size of the visible portion. We also know the distribution of sizes of the non-overlapped particles. Using this information we allocate a fraction of each overlapped rock to a small range of size classes that seems most likely given the visible portion of the overlapped rock.

In Figure 17 and Table 1 we show the results of sizing the fragments automatically identified in

Figure 13, and in Figure 18 and Table 2 we shows the sizing results for the fragments automatically identified in Figure 10.

4.8 *Three Days of Production*

Using the strategy outlined we processed 424 additional data sets for a LHD excavator across three days of production. We present the sizing results in Figure 19 in three subplots where the time of day is the horizontal axis. The top two subplots show the number of fragments of each size class in the same color scheme as the previous histograms. The number of rocks shown is the sliding window sum of five consecutive buckets. The bottom subplot shows the percentage of the visible surface that was classified as fines.

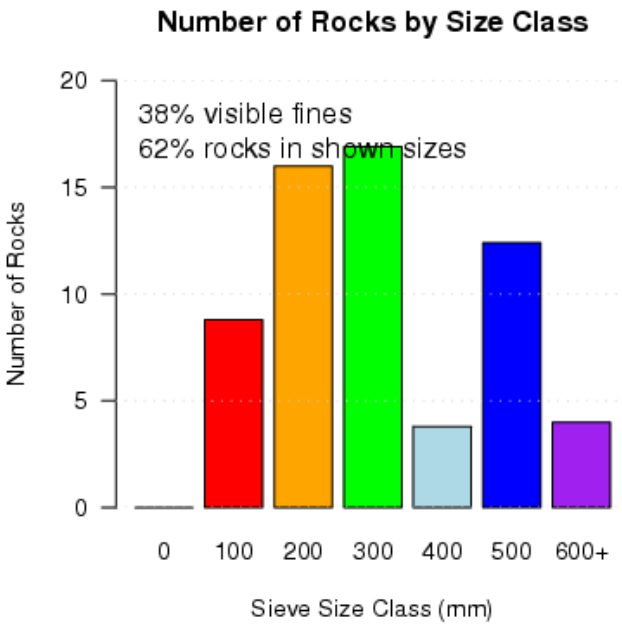

Figure 17. Sizing histogram (number of rocks by size class) for the fragments identified in Figure 13**.**

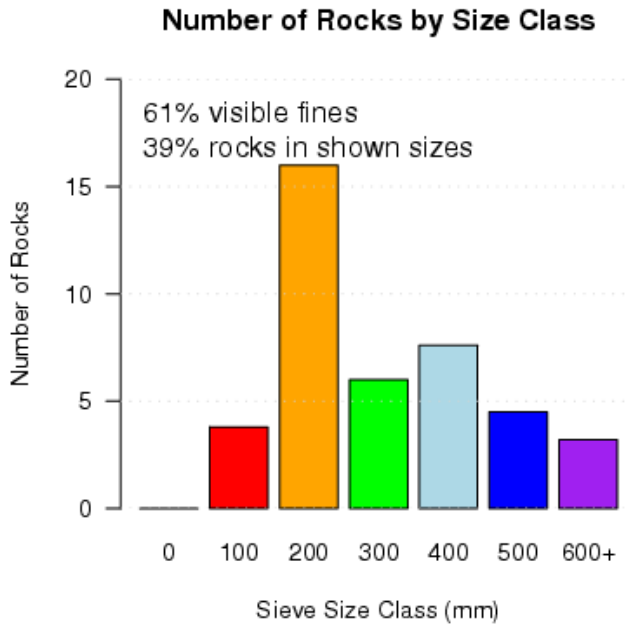

Figure 18. Sizing histogram (number of rocks by size class) for the fragments identified in Figure 10.

Table 1. Sizing results for Figure 13.

Size Classes					
100	200	300	400	500	600
15 Non-overlapped rocks					
5	3	2	0	4	1
47 Overlapped rocks					
3.8	13	14.9	3.8	8.4	3
Total of 62 measured rocks					
8.8	16	16.9	3.8	12.4	4
38% of the surface was classified as fines					

Table 2. Sizing results for Figure 10.

Size Classes					
100	200	300	400	500	600
6 Non-overlapped rocks					
2	4	0	0	0	0
35 Overlapped rocks					
1.8	12	6	7.6	4.5	3.2
Total of 41 measured rocks					
3.8	16	6	7.6	4.5	3.2
61.2% of the surface was classified as fines					

5 CONCLUSION

As a demonstration project the focus was proof-of-concept and in this respect the work has been very successful. The potential to capture 3D data of the passing LHD unit and perform automated analysis to identify and size the individual rock fragments has been demonstrated and shown to be achievable.

Furthermore a new ability to detect areas of fines has been developed that shows very promising results.

For the work to develop beyond this proof-of-concept stage there are a number of areas of the research that need further work in order to ensure robustness, accuracy and reliability. All of these tasks can be readily achieved.

- Further development and validation of the new fines detection algorithm.
- Classification boundaries for converting fragment best-fit-rectangle area into sieve size class need to be further investigated for this application.
- Conversion of the size distribution from “number of fragments” to a percentage by weight distribution is required and for this information about the ore being sized is necessary to give estimations for average fragment weight by size class for the material being measured. This encompasses the observation that particle shape varies as particle size changes.
- Investigation of what the observed proportion of fines on the surface can indicate about the fines in the overall mass and use this to produce a value for the 0-100mm size class in the percentage by weight distribution.
- Use observed surface proportions and knowledge of the bucket geometry to approximate the bucket size distribution. Supporting research has already been performed on laboratory rock piles in a cylindrical bucket (Thurley 2002).

6 ACKNOWLEDGEMENTS

Many thanks to ProcessIT Innovations, LKAB, and SoftcenterAB for their support, and participation.

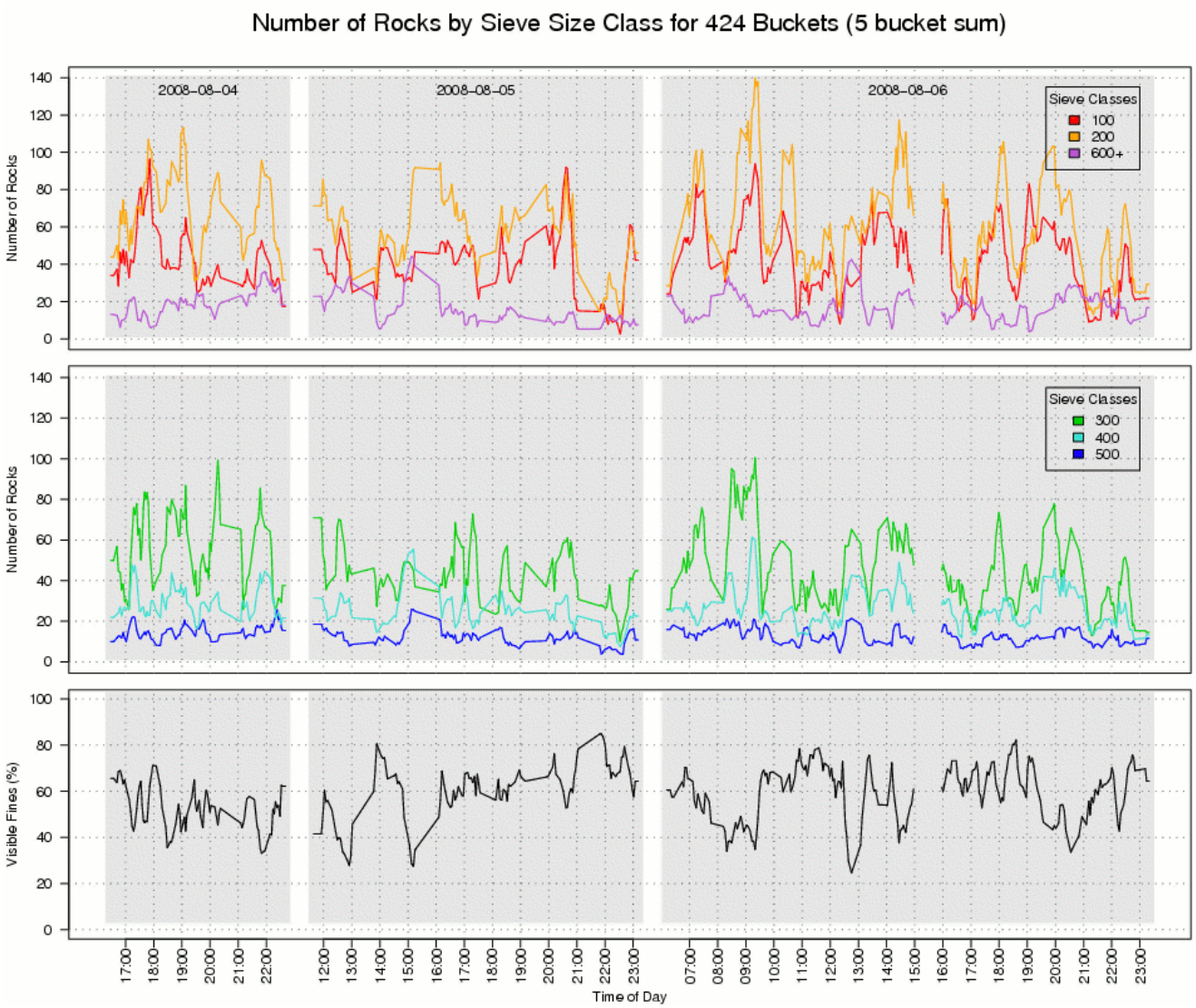

Figure 19. Number of rocks by sieve size class for three days of production (5 bucket sliding window summation).

REFERENCES

Carlsson, O. & Nyberg, L. 1983. A method for estimation of fragmentation size distribution with automatic image processing. In: *Proceedings of the First International Symposium on Rock Fragmentation by Blasting – FRAGBLAST*. Luleå, Sweden, August, pp. 333–345.

Frydendal, I. & Jones, R. 1998. Segmentation of sugar beets using image and graph processing. In: *ICPR 98 Proceedings – 14th International Conference on Pattern Recognition*. Vol. II. Brisbane, Australia, August, pp. 16–20.

Kim, H., Haas, C., Rauch, A. & Browne, C. 2003. 3D image segmentation of aggregates from laser profiling. *Computer Aided Civil and Infrastructure Engineering*: 254–263.

Lee, J., Smith, M., Smith, L. & Midha, P. 2005. A mathematical morphology approach to image based 3d particle shape analysis. In: *Machine Vision and Applications* 16(5): 282–288.

Noy, M.J. 2006. The latest in on-line fragmentation measurement - stereo imaging over a conveyor. In: *Proceedings of the Eighth International Symposium on Rock Fragmentation by Blasting – FRAGBLAST 8*. Santiago, Chile, May, pp. 61–66.

Potts, G. & Ouchterlony, F. 2005. The capacity of image analysis to measure fragmentation, an evaluation using split desktop. Tech. rep. Stockholm, Sweden: Swebrec - Swedish Rock Breaking Institute, ISSSN 1653-5006.

Thurley, M. & Andersson, T. 2007. An industrial 3d vision system for size measurement of iron ore green pellets using morphological image segmentation. *Minerals Engineering* 21(5): 405–415.

Thurley, M. & Ng, K. 2005. Identifying, visualizing, and comparing regions in irregularly spaced 3d surface data. *Computer Vision and Image Understanding* 98(2): 239–270.

Thurley, M. & Ng, K. 2008. Identification and sizing of the entirely visible rocks from segmented 3d surface data of laboratory rock piles. *Computer Vision and Image Understanding* 111(2): 170–178.

Thurley, M. J. 2002. Three dimensional data analysis for the separation and sizing of rock piles in mining. Ph.D. thesis, Monash University. Melbourne, Australia